Research Article | Vol. 26, No. 3 | 5 Feb 2018 | OPTICS EXPRESS 3161
Optics EXPRESS

Robust label-free biosensing using microdisk laser arrays with on-chip references

S. F. WONDIMU,[1,2,6] M. HIPPLER,[1,2,3] C. HUSSAL,[4] A. HOFMANN,[5] S. KRÄMMER,[3] J. LAHANN,[4] H. KALT,[3] W. FREUDE,[1,2] AND C. KOOS[1,2,*]

[1] *Institute of Microstructure Technology (IMT), Karlsruhe Institute of Technology (KIT), Hermann-von-Helmholtz-Platz 1, 76344 Eggenstein-Leopoldshafen, Germany*
[2] *Institute of Photonics and Quantum Electronics (IPQ), KIT, Engesserstr. 5, 76131 Karlsruhe, Germany*
[3] *Institute of Applied Physics (APH), KIT, Wolfgang-Gaede-Str. 1, 76131 Karlsruhe, Germany*
[4] *Institute of Functional Interfaces (IFG), KIT, Hermann-von-Helmholtz-Platz 1, 76344 Eggenstein-Leopoldshafen, Germany*
[5] *Institute of Applied Computer Science (IAI), KIT, Hermann-von-Helmholtz-Platz 1, 76344 Eggenstein-Leopoldshafen, Germany*
[6] *sentayehu.wondimu@kit.edu*
[*] *christian.koos@kit.edu*

Abstract: Whispering-gallery mode (WGM) microdisk lasers show great potential for highly sensitive label-free detection in large-scale sensor arrays. However, when used in practical applications under normal ambient conditions, these devices suffer from temperature fluctuations and photobleaching. Here we demonstrate that these challenges can be overcome by a novel referencing scheme that allows for simultaneous compensation of temperature drift and photobleaching. The technique relies on reference structures protected by locally dispensed passivation materials, and can be scaled to extended arrays of hundreds of devices. We prove the viability of the concept in a series of experiments, demonstrating robust and sensitive label-free detection over a wide range of constant or continuously varying temperatures. To the best of our knowledge, these measurements represent the first demonstration of biosensing in active WGM devices with simultaneous compensation of both photobleaching and temperature drift.

OCIS codes: (140.3945) Microcavities; (280.1415) Biological sensing and sensors; (280.3420) Laser sensors.

References and links

1. X. Fan, I. M. White, S. I. Shopova, H. Zhu, J. D. Suter, and Y. Sun, "Sensitive optical biosensors for unlabeled targets: A review," Anal. Chim. Acta **620**(1-2), 8–26 (2008).
2. M. Baaske and F. Vollmer, "Optical resonator biosensors: molecular diagnostic and nanoparticle detection on an integrated platform," ChemPhysChem **13**(2), 427–436 (2012).
3. M. A. Cooper, "Label-free screening of bio-molecular interactions," Anal. Bioanal. Chem. **377**(5), 834–842 (2003).
4. S. Krämmer, S. Rastjoo, T. Siegle, S. F. Wondimu, C. Klusmann, C. Koos, and H. Kalt, "Size-optimized polymeric whispering gallery mode lasers with enhanced sensing performance," Opt. Express **25**(7), 7884–7894 (2017).
5. T. Wienhold, S. Kraemmer, S. F. Wondimu, T. Siegle, U. Bog, U. Weinzierl, S. Schmidt, H. Becker, H. Kalt, T. Mappes, S. Koeber, and C. Koos, "All-polymer photonic sensing platform based on whispering-gallery mode microgoblet lasers," Lab Chip **15**(18), 3800–3806 (2015).
6. U. Bog, F. Brinkmann, H. Kalt, C. Koos, T. Mappes, M. Hirtz, H. Fuchs, and S. Köber, "Large-scale parallel surface functionalization of goblet-type whispering gallery mode microcavity arrays for biosensing applications," Small **10**(19), 3863–3868 (2014).
7. K. De Vos, I. Bartolozzi, E. Schacht, P. Bienstman, and R. Baets, "Silicon-on-Insulator microring resonator for sensitive and label-free biosensing," Opt. Express **15**(12), 7610–7615 (2007).
8. H. Li and X. Fan, "Characterization of sensing capability of optofluidic ring resonator biosensors," Appl. Phys. Lett. **97**(1), 011105 (2010).
9. D. K. Armani, T. J. Kippenberg, S. M. Spillane, and K. J. Vahala, "Ultra-high-Q toroid microcavity on a chip," Nature **421**(6926), 925–928 (2003).
10. L. He, Ş. K. Özdemir, and L. Yang, "Whispering gallery microcavity lasers," Laser Photonics Rev. **7**(1), 60–82 (2013).

#312276 https://doi.org/10.1364/OE.26.003161
Journal © 2017 Received 24 Nov 2017; revised 19 Dec 2017; accepted 19 Dec 2017; published 29 Jan 2018

Optics EXPRESS

11. J. Su, "Label-free single exosome detection using frequency-locked microtoroid optical resonators," ACS Photonics **2**(9), 1241–1245 (2015).
12. O. Scheler, J. T. Kindt, A. J. Qavi, L. Kaplinski, B. Glynn, T. Barry, A. Kurg, and R. C. Bailey, "Label-free, multiplexed detection of bacterial tmRNA using silicon photonic microring resonators," Biosens. Bioelectron. **36**(1), 56–61 (2012).
13. M. D. Baaske, M. R. Foreman, and F. Vollmer, "Single-molecule nucleic acid interactions monitored on a label-free microcavity biosensor platform," Nat. Nanotechnol. **9**(11), 933–939 (2014).
14. A. L. Washburn, L. C. Gunn, and R. C. Bailey, "Label-free quantitation of a cancer biomarker in complex media using silicon photonic microring resonators," Anal. Chem. **81**(22), 9499–9506 (2009).
15. J. T. Gohring, P. S. Dale, and X. Fan, "Detection of HER2 breast cancer biomarker using the opto-fluidic ring resonator biosensor," Sens. Actuators B Chem. **146**(1), 226–230 (2010).
16. A. Diaspro, G. Chirico, C. Usai, P. Ramoino, and J. Dobrucki, "Photobleaching," in *Handbook of biological confocal microscopy* (Springer, 2006), pp. 690–702.
17. L. Song, E. J. Hennink, I. T. Young, and H. J. Tanke, "Photobleaching kinetics of fluorescein in quantitative fluorescence microscopy," Biophys. J. **68**(6), 2588–2600 (1995).
18. G. D. Peng, Z. Xiong, and P. L. Chu, "Fluorescence decay and recovery in organic dye-doped polymer optical fibers," J. Lightwave Technol. **16**(12), 2365–2372 (1998).
19. G. Gupta, W. H. Steier, Y. Liao, J. Luo, L. R. Dalton, and A. K.-Y. Jen, "Modeling photobleaching of optical chromophores: light-intensity effects in precise trimming of integrated polymer devices," J. Phys. Chem. C **112**(21), 8051–8060 (2008).
20. Y. Huang, J. K. S. Poon, W. Liang, A. Yariv, C. Zhang, and L. R. Dalton, "Combined electromagnetic and photoreaction modeling of CLD-1 photobleaching in polymer microring resonators," Appl. Phys. Lett. **87**(7), 071108 (2005).
21. J. K. Poon, Y. Huang, G. T. Paloczi, A. Yariv, C. Zhang, and L. R. Dalton, "Wide-range tuning of polymer microring resonators by the photobleaching of CLD-1 chromophores," Opt. Lett. **29**(22), 2584–2586 (2004).
22. M. Iqbal, M. A. Gleeson, B. Spaugh, F. Tybor, W. G. Gunn, M. Hochberg, T. Baehr-Jones, R. C. Bailey, and L. C. Gunn, "Label-free biosensor arrays based on silicon ring resonators and high-speed optical scanning instrumentation," IEEE J. Sel. Top. Quantum Electron. **16**(3), 654–661 (2010).
23. J. T. Kirk, G. E. Fridley, J. W. Chamberlain, E. D. Christensen, M. Hochberg, and D. M. Ratner, "Multiplexed inkjet functionalization of silicon photonic biosensors," Lab Chip **11**(7), 1372–1377 (2011).
24. C. Lerma Arce, D. Witters, R. Puers, J. Lammertyn, and P. Bienstman, "Silicon photonic sensors incorporated in a digital microfluidic system," Anal. Bioanal. Chem. **404**(10), 2887–2894 (2012).
25. U. Bog, F. Brinkmann, S. F. Wondimu, T. Wienhold, S. Kraemmer, C. Koos, H. Kalt, M. Hirtz, H. Fuchs, S. Koeber, and T. Mappes, "Densely packed microgoblet laser pairs for cross-referenced biomolecular detection," Adv Sci (Weinh) **2**(10), 1500066 (2015).
26. L. He, Y. F. Xiao, C. Dong, J. Zhu, V. Gaddam, and L. Yang, "Compensation of thermal refraction effect in high-Q toroidal microresonator by polydimethylsiloxane coating," Appl. Phys. Lett. **93**(20), 201102 (2008).
27. N. Lin, L. Jiang, S. Wang, H. Xiao, Y. Lu, and H. Tsai, "Thermostable refractive index sensors based on whispering gallery modes in a microsphere coated with poly(methyl methacrylate)," Appl. Opt. **50**(7), 992–998 (2011).
28. H. K. Hunt and A. M. Armani, "Bioconjugation strategies for label-free optical microcavity sensors," IEEE J. Sel. Top. Quantum Electron. **20**(2), 121–133 (2014).
29. H. Y. Chen and J. Lahann, "Designable biointerfaces using vapor-based reactive polymers," Langmuir **27**(1), 34–48 (2011).
30. J. Lahann, I. S. Choi, J. Lee, K. F. Jensen, and R. Langer, "A new method toward microengineered surfaces based on reactive coating," Angew. Chem. Int. Ed. **40**(17), 3166–3169 (2001).
31. X. Deng, C. Friedmann, and J. Lahann, "Bio-orthogonal "double-click" chemistry based on multifunctional coatings," Angew. Chem. Int. Ed. Engl. **50**(29), 6522–6526 (2011).
32. U. R. Bog, "Optische Flüster-Galerie-Resonatoren und deren Funktionalisierung für die Biosensorik," Ph. D. (Karlsruhe Institute of Technology, Karlsruhe, 2015), pp. 79–110.
33. D. Doug, "Time pressure dispensing," White Papers, (Universal Instruments, 2009), http://www4. uic.com/wcms/WCMS2. nsf/index/Resources_58. html.
34. N. Tanaka and W. N. Sisk, "The photodegradation of pyrromethene 567 and pyrromethene 597 by pyrromethene 546," J. Photochem. Photobiol. Chem. **172**(2), 109–114 (2005).
35. C. E. Soteropulos, K. M. Zurick, M. T. Bernards, and H. K. Hunt, "Tailoring the protein adsorption properties of whispering gallery mode optical biosensors," Langmuir **28**(44), 15743–15750 (2012).
36. C. D. Heyes, J. Groll, M. Möller, and G. U. Nienhaus, "Synthesis, patterning and applications of star-shaped poly(ethylene glycol) biofunctionalized surfaces," Mol. Biosyst. **3**(6), 419–430 (2007).
37. H.-M. Haake, A. Schütz, and G. Gauglitz, "Label-free detection of biomolecular interaction by optical sensors," Fresenius J. Anal. Chem. **366**(6-7), 576–585 (2000).
38. P. Schuck, "Use of surface plasmon resonance to probe the equilibrium and dynamic aspects of interactions between biological macromolecules," Annu. Rev. Biophys. Biomol. Struct. **26**(1), 541–566 (1997).
39. M. A. Koussa, K. Halvorsen, A. Ward, and W. P. Wong, "DNA nanoswitches: a quantitative platform for gel-based biomolecular interaction analysis," Nat. Methods **12**(2), 123–126 (2014).

Optics EXPRESS

40. I. M. White and X. Fan, "On the performance quantification of resonant refractive index sensors," Opt. Express **16**(2), 1020–1028 (2008).
41. S. F. Wondimu, S. von der Ecken, R. Ahrens, W. Freude, A. E. Guber, and C. Koos, "Integration of digital microfluidics with whispering-gallery mode sensors for label-free detection of biomolecules," Lab Chip **17**(10), 1740–1748 (2017).
42. E. Hallynck and P. Bienstman, "Digital microfluidics with pressure-based actuation," IEEE Photonics Technol. Lett. **25**(17), 1656–1659 (2013).
43. I. Grimaldi, G. Testa, and R. Bernini, "Flow through ring resonator sensing platform," RSC Advances **5**(86), 70156–70162 (2015).

Introduction

Whispering-gallery mode (WGM) resonators show great potential for label-free molecular detection [1–3], combining high sensitivity [4] and micrometer-scale footprint [2] with the potential for cost-efficient mass production [5] and highly multiplexed sensing [6]. WGM resonators rely on rotationally symmetric geometries such as spheres, rings, capillaries, goblets and disks, in which light propagates along a convex outer contour and can evanescently interact with the surrounding medium [2, 7–9]. This interaction is resonantly enhanced over many round trips of the optical mode, thus leading to outstanding sensitivities that enable detection of single viruses and nanoscale particles [10, 11]. WGM-based sensors have found applications in life sciences for detection and quantification of proteins including oligonucleotides [12, 13] and cancer biomarkers [14, 15]. The desired output signal of WGM resonator sensors is a shift in resonance position due the attachment of biomolecules to the outer surface. Measurement of the resonance position in passive resonators relies on in-coupling of light from a tunable light source via evanescent coupling structures, and on recording of the transmission spectrum in which the resonance positions are marked with dips. Alternatively, active resonators doped with gain media like the microdisk lasers reported here can be excited and read out by free-space optics with sharp emission peaks marking resonance positions [6].

While WGM-based biosensors are intended to measure surface attachment of biomolecules, the resonance position is sensitive to all effects that lead to a refractive-index change of the resonator core and of the surrounding comprising, e.g., photobleaching of the gain medium or temperature fluctuations. The actual sensing signal is hence perturbed by a superposition of all these effects, thereby severely obstructing signal analysis. Photobleaching of the laser dye refers to the degradation of photoluminescence due to a decreasing concentration of photoactive chromophores. It is caused by an irreversible photochemical reaction of dye molecules and oxygen [16, 17]. As a consequence of photobleaching, the fluorescence emission decreases with time, thereby limiting device lifetime and performance. It has also been reported that photobleaching leads to a reduced refractive index of polymer-dye composites [18, 19], which results in a shift of the resonance positions to shorter wavelengths in WGM resonators. This effect has found applications in tuning the resonances of microring cavities doped with fluorescent dyes [20, 21]. However, the influence of photobleaching on the performance of WGM laser biosensors remains to be thoroughly investigated.

Another aspect that impairs the output signal of WGM-based biosensors is their sensitivity to temperature changes, caused by the thermo-optic effect of the core material and the physical expansion of the device. These effects have been investigated in the past and several approaches have been proposed to overcome it. For waveguide-based resonators, a common approach to cope with thermal drift during measurements is to use dedicated reference structures that are isolated from the analyte by a spin-coated passivation layer [22–24]. This approach, however, is only applicable to relatively flat structures of submicron height and is not suitable for high quality-factor resonators on elevated pedestals, for which spin-coating of a thick homogeneous passivation layer is challenging. For elevated resonators on pedestal structures, conformal coating of the reference device surface by a phospholipid film was demonstrated [25]. The viability of this approach was shown in a referenced sensing experiment, relying on a pair of size-mismatched adjacent microlasers, where one laser was functionalized while the other was passivated as a reference. In this experiment, temperature drifts

Optics EXPRESS

could be successfully compensated, but the effect of photobleaching was not addressed. Moreover, transfer of the phospholipid ink to the resonator surface requires highly sophisticated micro-contact stamping processes, in which a carefully aligned stamp pad must be brought into direct contact with the resonator surface without damaging the devices. These processes are delicate and hard to control, in particular when applied to extended arrays of resonators. Another approach to compensate temperature drift is based on hybrid resonator structures, where the resonators are coated with materials that have thermo-optic coefficients (dn/dT) that are opposite to that of the main resonator material, e. g., silica resonators ($dn/dT = 1.19 \times 10^{-5}$ /K) coated with a thin film of PDMS ($dn/dT = -1.0 \times 10^{-4}$ /K) [26,27]. This approach enables cancellation of temperature-induced wavelength drifts without the need for additional reference sensors, but it works only for a limited set of material combinations. In addition, the thickness of the applied film is a crucial parameter that must be carefully controlled. Moreover, temperature drift compensation by hybrid resonator structures has only been applied to passive devices so far.

In this paper, we report on a novel referencing approach for active resonators that can be applied to a wide range of structures including microdisks on elevated polymer pedestals. The approach is based on localized micro-dispensing of a passivation material and allows for simultaneous compensation of photobleaching and temperature drift. The deposition technique is applicable to a wide range of materials and device geometries and can be scaled to extended arrays of hundreds of devices. Functionality of the devices does not rely on any crucial geometrical parameter of the passivation layer that would need careful control. The viability of the concept is proven in a series of bio-sensing experiments, demonstrating reliable label-free detection over a wide range of constant or continuously varying temperatures. To the best of our knowledge, these measurements represent the first demonstration of biosensing in active WGM devices with simultaneous compensation of both photobleaching and temperature drift. The experiments could pave the path towards advanced lab-on-chip devices that allow a highly sensitive label-free detection outside well-controlled laboratory conditions.

Microdisk laser sensors

Operation principle

The basic structure of an active microdisk sensor is shown in Fig. 1. The device relies on a WGM laser cavity formed from a PMMA (poly(methyl methacrylate)) microdisk doped with a fluorescent dye (pyrromethene 597). Figure 1(b) shows the electric energy density of the laser mode. To excite the modes, the microdisk lasers are optically pumped via free-space optics, Fig. 2(a), using a pulsed laser emitting at a wavelength of 523 nm, which is in the absorption band of pyrromethene 597. The emission from the lasers is recorded by a spectrograph, and the lasing peaks of each laser are extracted and tracked by using a dedicated algorithm. In our biosensing experiments, we use chips with arrays of 16 lasers, Fig. 2(b), which are fixed in a flow cell. The chip is mounted on a sample stage, which allows for well-defined movements in a given sequence such that a specific selection of lasers can be repeatedly excited and measured. Easy addressing of individual microdisk lasers in arrays, a significant advantage of using free space optics, is an important feature that enables referenced sensing in this work.

Optics EXPRESS

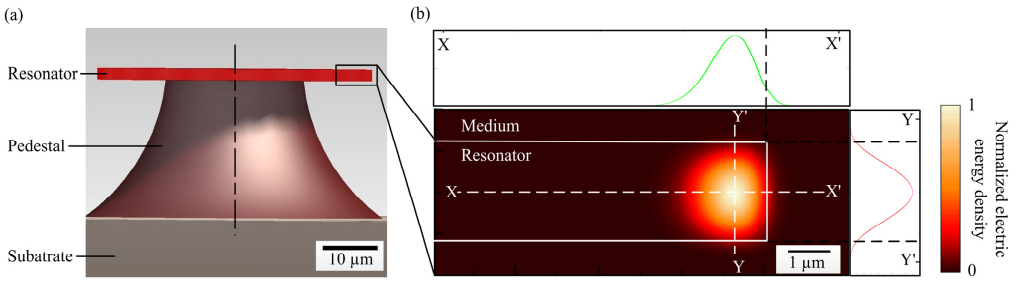

Fig. 1. Sensor principle. (a) Microdisk whispering-gallery mode resonator. The modes propagate along the convex outer contour of the disk. (b) Electric energy density distribution of the fundamental whispering-gallery mode. The electric field is predominantly oriented along the *y*-direction (E_y-mode). A certain part of the electric field interacts evanescently with the surrounding medium, enabling, e.g., detection of molecular binding to the resonator or surface. Profiles of the energy density along the diameters XX' and YY' are shown in the graphs.

An important requirement for WGM lasers to operate as biosensors is their selectivity to a given target molecule. This is accomplished by covalent binding of receptor molecules to the resonator surface by using a click-chemistry-based functionalization protocol. Covalent functionalization approaches are known to be more stable and controllable than approaches based on physical adsorption [28, 29]. Since PMMA lacks active functional groups, the surface was activated prior to functionalization by chemical vapor deposition (CVD) of pentafluorophenyl ester (pfp-ester) acting as reactive coating. For compensation of temperature drift and photobleaching, a selection of sensors was passivated by local deposition of a low-refractive index adhesive that entirely covers the respective structure, Fig. 2(b). This passivation approach can be applied to a wide variety of material platforms and resonator structures, comprising microdisks on elevated pedestals.

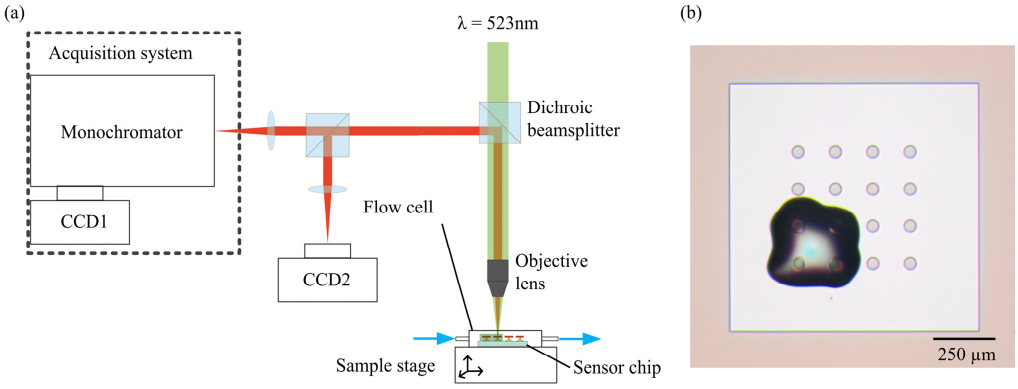

Fig. 2. Measurement setup. (a) The microdisk lasers are pumped from the top by a frequency-doubled pulsed Nd:YLF laser emitting at 523 nm. The beam is focused by a microscope objective (20 × , NA = 0.42). The sensor chip is fixed in a flow cell mounted on an automated sample stage, which allows for well-defined movements in a given sequence such that a specific selection of lasers can be repeatedly pumped and measured. The emission from the microdisk lasers is collected through the same objective lens and is directed to the acquisition system. The acquisition is done by a Czerny-Turner monochromator (Shamrock 500i, Andor) equipped with a CCD camera (CCD 1, iDus, Andor). Part of the emission is directed to another camera (CCD 2) to monitor the position of the microdisks. (b) Image of the sensing area from the top showing 16 microdisk lasers. The reference sensors are covered by the applied passivation layer (darker shade), which physically seals them thereby avoiding interaction with the analyte.

Optics EXPRESS

Fabrication

The fabrication process of the sensor array is illustrated in Fig. 3 and is similar to the processes described in [5]. In a first step, two layers are subsequently spin-coated onto a silicon base wafer. The first layer consists of 5 µm-thick PMGI (polymethylglutarimide, MicroChem Corp.) and is covered by a second 1.2 µm-thick film of PMMA (MicroChem Corp.) mixed with pyrromethene 597 (Radiant Dyes Laser & Accessories GmbH). Electron beam lithography followed by development of the PMMA layer in a 1:1 mixture of methyl-isobutyl-ketone (MIBK) and isopropanol (IPA) was used to structure an array of disks. Subsequent isotropic wet etching of the PMGI layer with 101A developer (MicroChem) was used to underetch the disks and to form pedestals thus freeing the edges of the disks where the whispering-gallery modes can propagate. Note that this technique allows for fabrication of high-Q WGM resonators without using a reflow process, which is often exploited to smoothen the surface after fabrication. Reflow processes can lead to variations of the resonator size and hence the sensitivity within a sensor array. Note also that electron-beam lithography was only used due its flexibility in changing the device layout. The disks can also be structured with low-cost mask-based UV lithography without impairing the performance [5].

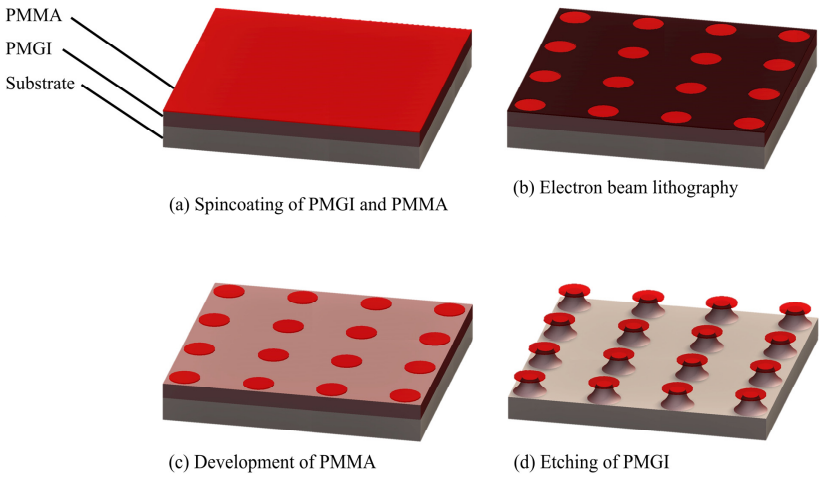

Fig. 3. Fabrication of microdisk lasers. (a) PMGI and dye-doped PMMA are spin-coated subsequently on a silicon base wafer. (b) Disks are structured in the PMMA layer by electron-beam lithography. (c) Disks are formed by developing the exposed PMMA layer. (d) Selective etching of the PMGI layer forms pedestals, thus freeing the edges of the disks where the whispering-gallery modes can propagate.

Surface activation

For covalently attaching the receptor molecules, the resonator surface needs to be activated by depositing pfp-ester in a CVD process, see Fig. 4(a). To this end, we start from synthesizing [2.2] paracyclophane-4-carboxylic acid pentafluorophenyl ester **(1)**, which acts as a precursor for the pfp-ester, see [30] for details of the synthesis and the deposition. The precursor **(1)** was sublimated at temperatures between 120 and 130°C under low pressure (< 0.1 mbar) before entering a pyrolysis furnace. The furnace was maintained at 560°C, with an argon flow of 20 sccm (standard cubic centimeter per minute), to induce the cleavage into two reactive monomers (quinodimethanes, **(2)**). The reactive monomers were guided into the deposition chamber, where the sensor chips were kept at a rather low temperature of 15°C to enhance adhesion of monomers to the device surface, followed by an in situ polymerization reaction [29–31]. The argon flow rate was chosen for a deposition rate of 5 nm/min, and the process was run for 30 min. The resulting layer **(3)** has active pfp-ester groups (shown in red) and forms a homogeneous 150 nm-thick conformal coating on the sensor surface. The thickness

Optics EXPRESS

of 150 nm was chosen based on previous work [32], which aimed at optimizing the coating for maximum sensitivity. The thickness of the fabricated layers was confirmed by ellipsometry (J. A. Wollam M-44, LOT-Quantum Design GmbH). Surfaces terminated with pfp-ester can be functionalized via click-chemistry allowing attachment of a wide variety of receptor molecules terminated with amino groups [30]. Moreover, the CVD deposited reactive polymer is proven to have excellent adhesion on a multitude of materials so that it can be universally applied on sensors structured from various materials [30].

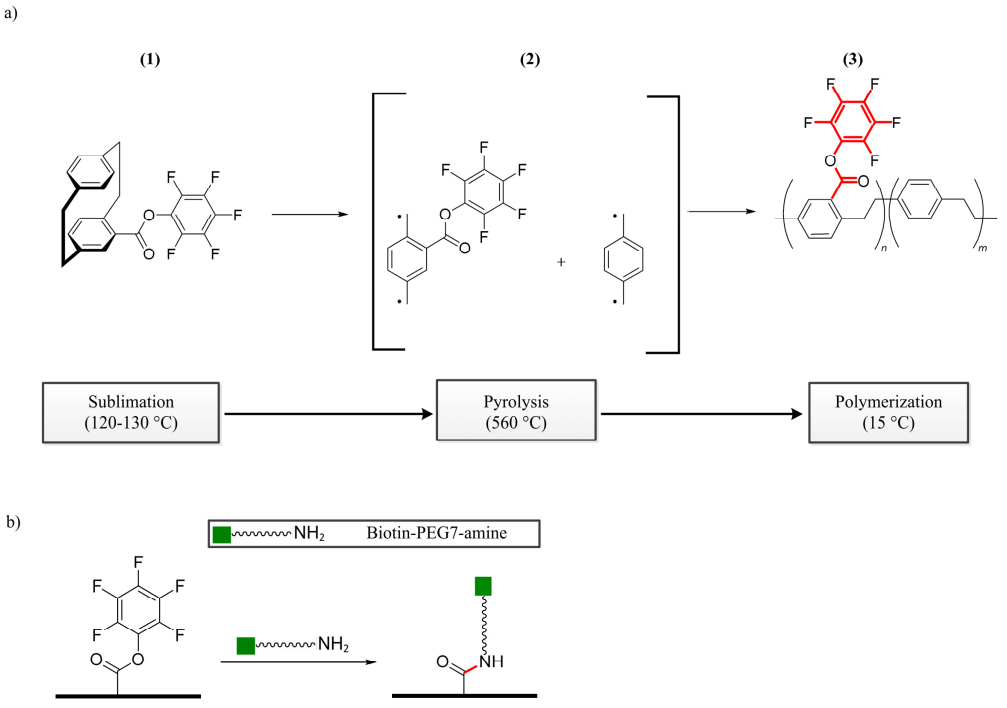

Fig. 4. Surface activation and functionalization. (a) The surface of the microdisk lasers is activated by deposition of pentafluorophenyl- ester (pfp-ester). The precursor ([2,2] paracyclophane-4-carboxylic acid pentafluorophenyl ester, **(1)**) is sublimated and guided through a pyrolysis chamber where it breaks into two reactive monomers **(2)**. The monomers are then directed to the surface of the cooled sensor chips for in situ polymerization **(3)**. (b) The resonator surface was biotinylated to allow specific binding of streptavidin. The biotin is terminated with an amine group, which reacts with the pfp-ester forming a covalent amide bond (shown in red).

After application of the activation layer, the lasing threshold increased from 15 nJ/pulse to 86 nJ/pulse, indicating that surface activation reduces the quality factor of the resonators. However, this change does not significantly affect the detection limit of our acquisition system: The lasing linewidth is well below the resonance linewidth of the cavity and also well below the resolution limit of our spectrometer, which displays a resolution-limited 30 pm-wide spectral peak before and after surface activation.

Passivation concept

Reference sensors were passivated by localized deposition of a UV-curable adhesive (MY136 V2000, MYpolymers LTD, Isreal). This material has a refractive index of $n = 1.37$, which is smaller than the one of our resonator core ($n = 1.49$). This is an important requirement for WGM modes to propagate. Note that only a tiny portion of the guided light (approx. 5% of

Optics EXPRESS

the modal power) propagates outside the PMMA core, i.e., in the analyte or the passivation layer. Thermal drift is hence dominated by the thermo-optic coefficient of the PMMA core such that a mismatch of the thermo-optic coefficients of the analyte and the passivation layer can be neglected. The deposition was performed in two layers (two sequences) to ensure a thick coverage of the reference elements, such that interaction of the optical modes of the reference sensors with the analyte is safely avoided. Figure 5(a) shows sketch of the dispensing system. The sensor chips were vacuum-clamped on a high precision manipulation platform based on a Smarpod 110.45 manipulator with three linear axes and three rotary axes (Smarpod 110.45, SmarAct GmbH). Glass needles were then used for highly precise local dispensing of the UV-curable adhesive that acts as a thick passivation layer. Close-up images of the needle and sensor chip are shown in Fig. 5(b) and 5(c). The application of the adhesive was done with a time pressure dispensing workstation (Ultimus II, Nordson EFD). Time pressure dispensing relies on applying pressure to the glass needle, where the pressure pulse is controllable and allows for repeatable dispensing of the adhesive [33]. We work under low dispensing pressure utilizing the wetting behavior of the substrate and the microdisk. The adhesive was cured after each dispensing step in a nitrogen environment using an LED-based

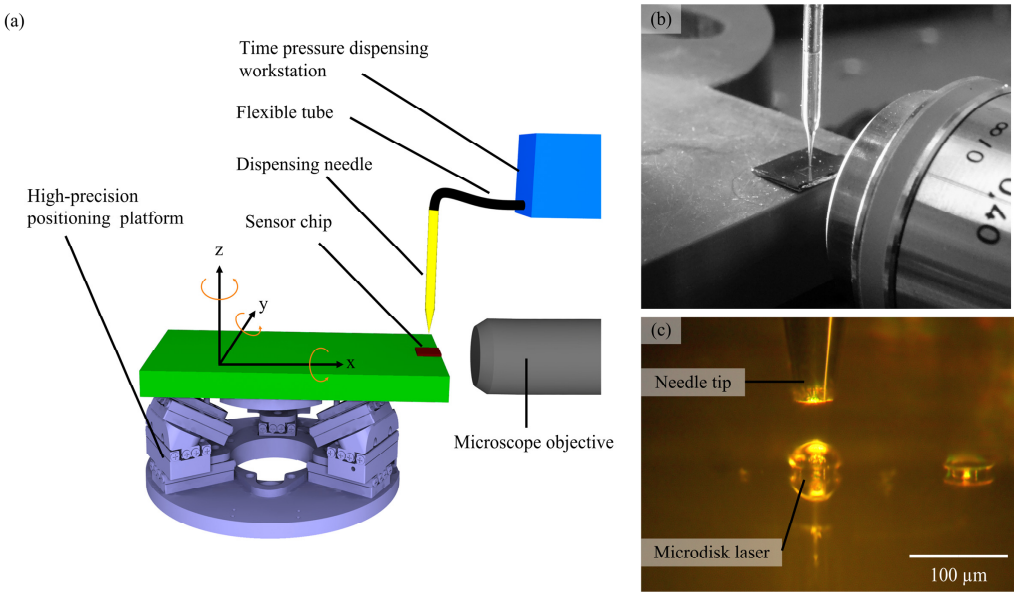

Fig. 5. Passivation setup. (a) The sensor chips were mounted on a high-precision positioning platform (Smarpod 110.45, SmarAct GmbH) with six degrees of freedom. Reference resonators were selectively passivated by localized dispensing of a low-refractive index adhesive through a thin glass needle which was fixed on a mount (not shown here for simplicity). The application of the adhesive was done with a time pressure dispensing (Ultimus II, Nordson EFD) workstation connected to the needle through a flexible tube. A horizontal microscope was set up to monitor the dispensing from the side. (b) Close-up image of the dispensing system showing a partially filled needle over a sensor chip. (c) Optical image acquired by the horizontal microscope, showing the needle tip close to a microdisk laser covered by dispensed passivation material.

UV curing system (365nm LED head, Aicure UJ35, Panasonic). Curing under nitrogen minimizes any UV-induced degradation of the organic dye by minimizing the concentration of oxygen [34]. The output power of the curing lamp was set to approximately 1.2 W/cm^2 on the surface of the sensor chips, with 15 seconds of curing time for each dispensing step. The passivating and curing process did not have a significant effect on the lasing threshold of the lasers.

Optics EXPRESS

Surface functionalization

In order to demonstrate the referencing capability of our sensors in biosensing measurements, we monitored the binding of streptavidin to sensors functionalized with biotin. For functionalization of CVD-activated sensor chips, we incubated them in a solution of 500 µM amine-PEG7-biotin (Celares GmbH) for 24 hours. The activated ester groups on the surface of the chips react with the amine group (NH_2). The PEG units orient the biotin outwards in addition to minimizing non-specific attachment of molecules to the surface of the sensors [35, 36].

Measurement results and discussion

Effects of photobleaching and temperature change

Our referencing scheme depends crucially on identical responses of the measurement devices and of the reference elements with respect to temperature fluctuations and photobleaching. This is confirmed in a first set of experiments, which were all performed in an aqueous environment. We simultaneously measure emission spectra of a passivated reference laser and a functionalized measurement laser, and track the spectral positions of the lasing peaks over time. A first set of measurements is geared towards investigating the effect of photobleaching, and was run under constant temperature. Figure 6(a) shows the resulting shifts in emission peak positions over time. The reference and measurement lasers showed identical shifts to shorter wavelengths, which can be assumed linear during the measurement period. In a second set of experiments, the response of the sensor chips to temperature fluctuations was investigated, see Fig. 6(b). A Peltier cooler integrated into the flow cell was used to change the temperature, which was monitored by a PT100 resistive temperature detector (RTD) mounted inside the flow cell. As shown in Fig. 6(b), the reference and measurement sensors showed identical responses to the temperature change of the flow cell. After correction for photobleaching, the temperature sensitivity of the resonators was determined to be –30 pm/K.

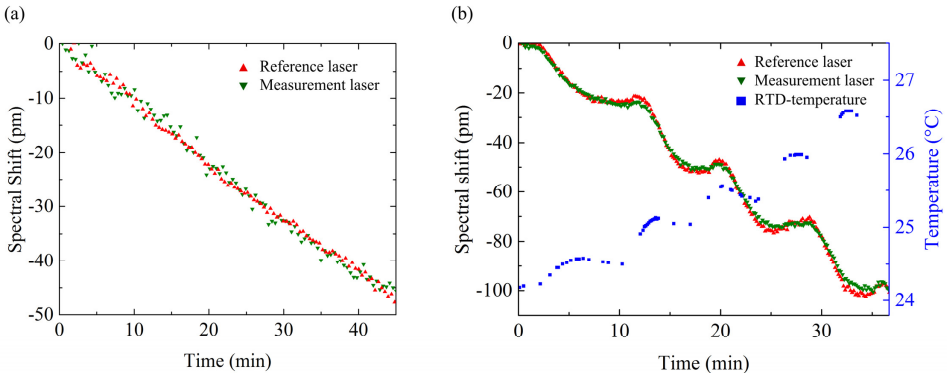

Fig. 6. Responses to bleaching and temperature change as obtained from two lasers on a common chip. The reference laser is covered by the locally dispensed passivation material. (a) Identical spectral shifts induced by photobleaching were recorded for the reference and measurement lasers. (b) Similar trends were recorded in spectral shift when the lasers were subjected to temperature changes.

The fact that the reference and measurement sensors show identical responses to photobleaching and temperature variation is a key criterion for the implementation of on-chip referencing. The shift of the measurement lasers contains all the information about photobleaching, temperature drift and surface biomolecule binding, whereas the reference lasers show shifts only to photobleaching and temperature drift. Hence, the recorded data can be corrected and accurate binding curves can be obtained by subtraction of spectral shift of the reference from that of the measurement laser.

Optics EXPRESS

To prove that the reference sensors are not affected by the presence of the analyte, we perform a measurement at a constant temperature, see Fig. 7. Streptavidin (1 ml, 12 µg/ml in PBS) was injected into the flow cell at t = 0 min for one minute, and the spectral shifts of the reference and measurement lasers were measured. A binding-related spectral shift is only observed for the measurement sensor but not for the reference device. We conclude that the passivated reference sensors are buried under a sufficiently thick passivation layer and the guided light does hence not interact with the analyte. The residual linear blue shift of the reference sensor is attributed to photobleaching. Note that our passivation approach only compensates for photobleaching-induced spectral shifts, but does not prevent photodegradation of the lasing intensity itself. Therefore, the signal-to-noise ratio of our measurements decreases continuously with measurement time. For a fair comparison, we stopped all experiments after 30 min.

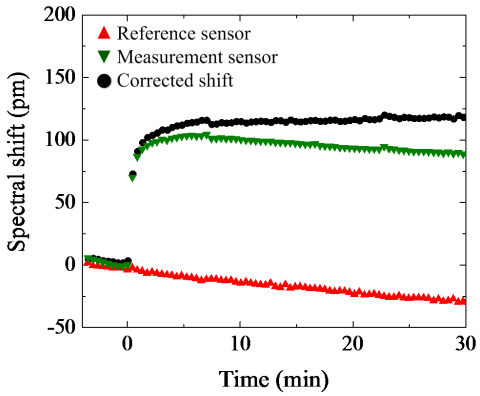

Fig. 7. Referenced sensing principle. The binding of streptavidin was recorded under constant temperature. The spectral shift of the measurement sensor is caused by photobleaching and binding of biomolecules to the surface, whereas the reference laser shows a shift due to photobleaching only. The corrected shift is obtained by subtracting the spectral shift of the reference from that of the measurement laser. The measurements do not show any influence of the analyte on the reference sensors, confirming that the devices are buried sufficiently deep in the passivation layer to prevent interaction of the guided light with the analyte.

Referenced biosensing under simulated temperature disturbances

After confirming identical responses of the reference and measurement sensors to temperature drift and photobleaching, we evaluate the performance of the sensors under simulated temperature fluctuations with a target biomolecule present. To this end, the binding of streptavidin to functionalized sensors was recorded while the temperature of the flow cell was randomly altered during the experiment. The maximum rate of temperature change was 0.16 K/min. This rate corresponds to a temperature change of approximately 5 K within the 30 minutes of the binding measurements. This is a realistic rate of temperature change under normal ambient conditions. The measurement results are shown in Fig. 8. At the beginning of the experiment, streptavidin (1 ml, 12 µg/ml in PBS) was injected into the flow cell for one minute, and the spectral shifts of the reference and measurement lasers were measured. The temperature of the flow cell was recorded with a PT-100 resistance temperature detector (RTD) for control. The spectral shift of the reference laser (shown in red) shows a response only to temperature drift and bleaching. The measurement laser (shown in green), on the other hand, shows a response to the binding of streptavidin in addition. The corrected shift (shown in black) is obtained by subtraction of the spectral shift of the reference laser from that of the measurement laser. After 30 minutes of measurement, the wavelength shift Δ caused by the combination of the temperature drift and photobleaching accumulates to approximately –40

Optics EXPRESS

pm and is comparable to the detection signal. This underlines the importance of reliable referencing schemes.

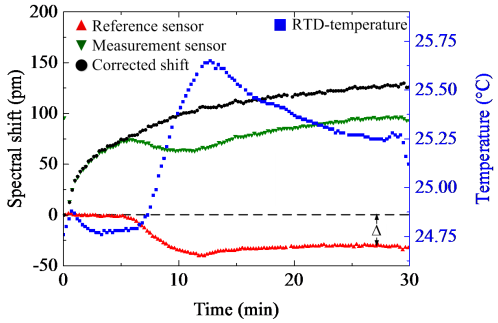

Fig. 8. Referencing of measurements. The binding of streptavidin to biotinylated resonator surfaces was recorded under simulated environmental condition with temperature variations. The reference sensor (red trace) was passivated and is hence only sensitive to temperature fluctuations and photobleaching. The measurement sensor (green trace) showed a wavelength shift affected by the changing environment conditions, which overlays the wavelength shift resulting from the normal binding kinetics. The measured data was corrected by subtraction of the reference data to obtain the actual molecular binding response (black trace).

Stability at elevated temperatures

Besides temperature fluctuations during measurements, the absolute sensor temperature is a possible source of disturbance to the sensor response. To investigate this aspect, measurements were performed at different constant ambient temperatures. To this end, the temperature of the flow cell was stabilized by a closed-loop control during streptavidin detection. Figure 9 shows the measured wavelength shift evolution for a 6 µg/ml streptavidin solution in PBS at different ambient temperatures. The resulting shifts after 30 minutes did not show any systematic dependence on operating temperature. The resulting average shift was 85.2 ± 3.8 pm. We stopped all measurements after 30 min to prevent excessive degradation of the signal-to-noise ratio due to photobleaching. The residual slope of the spectral shift at 30 min appears pretty consistently for all measurements and is attributed to the actual binding kinetics of the analyte to the functionalized surface, possibly in combination with non-specific binding. It is also observed in Fig. 10(a).

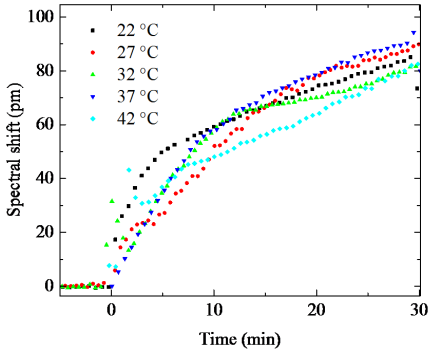

Fig. 9. Effects of the environmental temperature on the sensor signal. The binding of a fixed concentration of streptavidin (6 µg/ml) was measured with several chips, operated at different temperatures between 22°C and 42°C. All temperatures were kept constant during each measurement. The measured chips show nearly identical final shifts after a duration of 30 minutes, the time used for the sensing experiments. The variations for the curves after injection of the analyte at $t = 0$ are attributed to initial temperature differences between the streptavidin solution and the heated chips. The final spectral shift of the sensors after 30 minutes is 85.2 ± 3.8 pm – at this time, the solution has warmed up to the same temperature as the chips.

Optics EXPRESS

For confirming the independence of the resulting shifts on temperature, we compared the uncertainty of the final spectral shifts with the theoretical estimate. We used the simple molecular binding model to calculate the effect of temperature change on the shift of the sensors [37, 38]. According to this model, the resulting shift $\Delta\lambda$ for the attachment of target molecules of concentration C is given by

$$\Delta\lambda = \Delta\lambda_{\max}\left(1+\frac{k_{\text{off}}}{Ck_{\text{on}}}\right), \quad (1)$$

where $\Delta\lambda_{\max}$ is the expected shift when all the binding sites are occupied. The quantities k_{on} and k_{off} are temperature-dependent association and dissociation rate constants for the binding molecules of interest. For our estimation, we use values of k_{on} and k_{off} for streptavidin-biotin binding at different temperatures reported by Koussa *et al.* [39]. For the concentration of 6 µg/ml under investigation, a temperature increase by 20 K would cause a relative change $\delta\lambda$ of the wavelength shift $\Delta\lambda$ of $\delta\lambda/\Delta\lambda = 10^{-5}$. This deviation is insignificant in comparison to the standard deviation in determining the peak position wavelengths (0.45 pm), which is limited by the resolution of the spectrometer. Temperature-dependent shifts can hence be safely neglected for biotin-streptavidin binding.

Biosensing demonstration and sensitivity analysis

In order to quantify the sensitivity of the devices to streptavidin, their response to varying streptavidin concentrations was recorded; see Fig. 10(a). Streptavidin solutions were injected at time t = 0 min and the sensors were incubated in the solution for 30 minutes. The accumulated spectral shifts averaged over the last 5 minutes (grey background) were used to plot the curve in Fig. 10(b) and to determine the sensitivity and detection limit. As shown in Fig. 10(b), the accumulated wavelength shifts of the sensors show a non-linear dependence on streptavidin concentration, which was fit to a Hill model (squared correlation coefficient R^2 = 0.997). The maximum sensitivity of the sensors can be determined from the linear part by calculating the slope. This results in a sensitivity of S = 13 pm/(µg/ml) – the highest value so far reported for active WGM resonators. Based on the standard deviation σ = 0.45 pm of

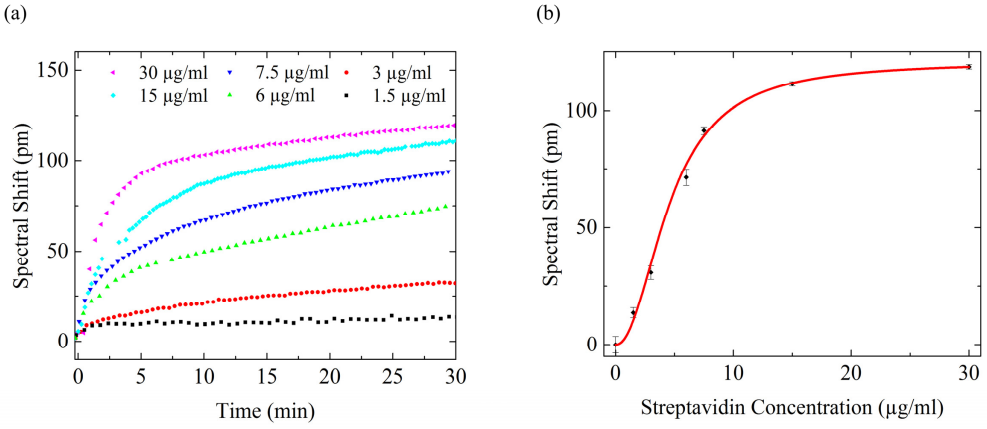

Fig. 10. Biosensing demonstration and sensitivity analysis. (a) Binding curves for different concentrations of streptavidin on biotinylated lasers. (b) Accumulated wavelength shifts for the different concentrations, obtained from averaging over the grey shaded regions in (a). The data were fit by a curve obtained from the Hill model (R^2 = 0.997). From the linear part of the measured data, we obtain a sensitivity of 13 pm/(µg/ml).

the resonance wavelengths, limited by the spectrometer, the determined sensitivity corresponds to a detection limit [40] $\delta = 3\sigma/S$ of 104 ng/ml for streptavidin binding. Note that due

Optics EXPRESS

to the temperature sensitivity measurements (–30 pm/K), a temperature fluctuation by only 0.1 K would already result in a wavelength shift of 3 pm, which would increase worsen the detection limit by a factor of more than six. This highlights the importance of the referencing scheme.

Note that the detection limit of 104 ng/ml is the best value so far obtained for active WGM sensors, outperforming the 134 ng/ml demonstrated in previous experiments, for which photo-bleaching had to be avoided by small pump powers. These experiemnts were also based on rather complex fabrication techniques, involving reflow processes to smoothen the WGM surfaces as well as aligned micro-contact stamping for local deposition of passivation layers [25]. Our present results can be further improved, e.g., through optimized surface functionalization with higher density of receptor molecules, through increasing the overlap of the resonant modes with the surrounding by optimizing resonator dimensions [4], or through advanced data acquisition and processing techniques which are subject of further studies.

Conclusions and outlook

Temperature changes and photobleaching were identified as major impairments of active WGM biosensors, rendering operation of these devices challenging outside a controlled laboratory environment. This can be overcome by a referencing scheme that relies on passivated sensors in addition to functionalized measurement sensors. The approach is based on localized micro-dispensing of passivation material on top of WGM lasers, and is well suited for extended arrays of hundreds of devices. Proof-of-concept experiments carried out under simulated environmental conditions demonstrate the viability of the concept. To the best of our knowledge, these measurements represent the first demonstration of biosensing in active WGM devices with simultaneous compensation of both photobleaching and temperature drift. Both the detection limit of 104 ng/ml and the sensitivity of 13 pm/(µg/ml) represent the best values so far obtained for active WGM resonators. Further improvements are possible by optimizing the functionalization protocol to achieve higher density of receptor molecules, or by optimizing resonator dimensions to increase the overlap of the resonance modes with the surrounding [4]. Furthermore, active analyte agitation during measurements can accelerate response times, for example by using digital microfluidics or continuous flow systems [41–43]. In the future, the concept of localized dispensing may be extended to selective functionalization of resonators within a large-scale array to enable simultaneous detection of multiple target molecules.

Funding

Alfried Krupp von Bohlen und Halbach Foundation; European Research Council (ERC Starting Grant ‘EnTeraPIC’, number 280145); State graduate fund (Landesgraduiertenförderung) Baden-Württemberg, Germany; Carl Zeiss Foundation; Karlsruhe School of Optics and Photonics (KSOP).

Acknowledgments

This work was carried out with the support of the Karlsruhe Nano Micro Facility (KNMF), a Helmholtz Research Infrastructure at Karlsruhe Institute of Technology.